第26卷第6期
2011年11月

热　能　动　力　工　程
JOURNAL OF ENGINEERING FOR THERMAL ENERGY AND POWER

Vol. 26, No. 6
Nov. ,2011

文章编号:1001-2060(2011)06-0756-05

基于TMS320C31+FPGA数字控制器的主被动磁悬浮飞轮一体化控制

张福鑫,李光军,刘　刚,文　通
(北京航空航天大学 仪器科学与光电工程学院,北京 100191)

摘　要:针对轴向三自由度被动、径向两自由度主动控制的主被动磁悬浮飞轮的低功耗、高可靠、一体化需求,对其控制器进行了一体化设计。首先,建立了主动磁轴承的数学模型,并选择合适的控制策略。在此基础上,提出一种以DSP+FPGA为核心,包含信号调理、外部存储、驱动及功放模块的一体化集成数字控制系统,并对其进行实验验证。实验结果表明,飞轮在静态悬浮时,转子径向跳动量为70 mV左右,约为保护间隙(峰-峰值约8 V)8.7%;加速至额定转速时,转子跳动量为1.2 V左右,约为保护间隙的15%左右,磁悬浮飞轮以额定转速工作时磁轴承系统功耗为5.5 W,满足飞轮性能要求。

关 键 词:主被动磁悬浮飞轮;磁轴承;一体化控制器;DSP;FPGA

中图分类号:TH133.7　　**文献标识码**:A

引　言

磁悬浮飞轮(Magnetic Suspending Flywheel,MSFW)是卫星姿态控制的主要执行部件,它通过控制转子的转速改变输出角动量,产生控制力矩,从而改变卫星的姿态,具有低功耗、高转速、小体积等优点[1~2],其输出控制力矩的精度决定了卫星的姿态稳定[3~4]。主被动磁悬浮飞轮轴向采用被动磁轴承、径向采用主动磁轴承,从而达到对轴向三自由度、径向两自由度精确控制的目的。此种结构具有结构简单、精度高、可靠性高等特点[5],是航天器姿态控制的新型支撑技术。

磁轴承分为纯电磁式磁轴承和永磁偏置加电磁控制的混合磁轴承。与纯电磁式磁轴承相比较,混合磁轴承中永磁磁场提供承载力,电磁磁场起调节作用,因此控制电流显著减小,降低损耗[6]。磁轴承控制器是主被动磁悬浮飞轮控制系统的核心,其控制性能的好坏直接影响到整个系统的稳定性及控制精度。数字控制器相对模拟控制器易于实现先进控制算法以及高精度控制策略,并且具有功耗低、体积小、适合集成化的优点。因此磁轴承控制系统采用DSP+FPGA的数字控制模式,有效地减小控制电路的体积、重量并提高控制系统的可靠性。

现有的全主动磁悬浮飞轮在五个自由度上全部采用主动磁轴承,为了减小进动和章动两个涡动模态对转子系统稳定性的影响,引入基于分散PID的滤波交叉反馈控制算法,增加了控制系统的运算量,单一DSP+FPGA无法满足,因此采用双DSP+FPGA方案分别实现对电机和磁轴承的控制。主被动磁悬浮飞轮只有径向两自由度采用主动磁轴承,因此在控制算法相对简单,一套DSP+FPGA就可以同时实现对电机和磁轴承的控制,因此设计了一种以DSP+FPGA为核心、包括信号调理模块、驱动及功率放大模块、外部存储模块的电机-磁轴承一体化集成数字控制系统,并对其进行实验验证。

1　磁轴承控制系统建模

主被动磁悬浮飞轮径向采用主动磁轴承进行控制,其结构如图1所示,假设转子为刚性转子,电磁力和控制电流、转子位移在其工作点附近成近似线性关系,功放单元等效为理想一阶低通滤波器,控制器单元为不完全微分PID控制器,信号调理单元等效为理想二阶低通滤波器。转子的实际位移由电涡流位移传感器进行测量,电涡流位移传感器是基于导体的电涡流效应制成的[7],具有集成度高,稳定性好,抗干扰性强等优点[8]。

建立质心坐标系O-XYZ,转子沿X、Y轴两个主动自由度上动力学方程为:

$$\begin{cases} m\ddot{x}=f(x) \\ m\ddot{y}=f(y) \end{cases} \tag{1}$$

经普拉斯变化后可得:

收稿日期:2011-06-13;　**修订日期**:2011-07-03

作者简介:张福鑫(1985-),男,黑龙江哈尔滨人,北京航空航天大学硕士研究生.

?1994-2018 China Academic Journal Electronic Publishing House. All rights reserved.　http://www.cnki.net

$$\begin{cases} ms^2X(s) = F_X(s) \\ ms^2Y(s) = F_Y(s) \end{cases} \tag{2}$$

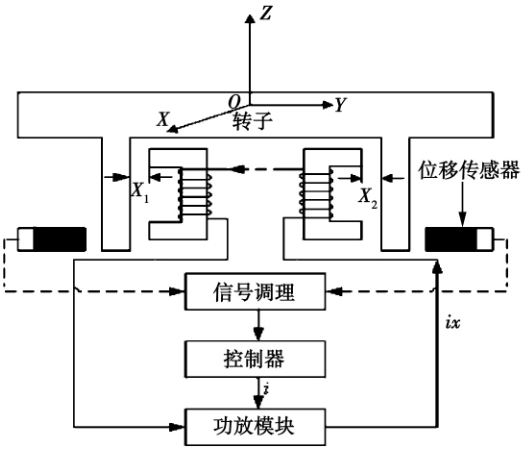

图 1　径向主动磁轴承示意图

Fig. 1 Schematic drawing of a radial driving magnetic bearing

经过线形化的磁轴承力为:

$$f(x) = K_X \cdot X + K_i \cdot i_X \tag{3}$$

拉普拉斯变化后可得:

$$F_X(s) = K_X \cdot X(s) + K_i \cdot I_X(s) \tag{4}$$

式中: K_i—电流刚度矩阵; K_x—位移刚度矩阵; X—磁轴承转子位移; i—控制量输入。

由于 PID 控制算法具有算法简单、鲁棒性好、可靠性高的优点,所以主动磁轴承采用 PID 控制器[9],但是传统的 PID 控制算法存在微分项不足的缺点,因此在原有的 PID 控制算法中加一个惯性环节 $1/(1+T_f s)$,构成不完全微分 PID,其传递函数为:

$$G(s) = I(s)/E(s) = K_p(1 + 1/T_i s + T_d s/(1 + T_f s)) \tag{5}$$

其中,$e = \triangle X = X - X_0$,$X_0$ 为转子平衡位置,X 为传感器测量的转子实际位置,由式(5)可以推导出:

$$I(s) = K_p \cdot E(s) \cdot \left(1 + \frac{1}{T_i s} + \frac{T_d s}{1 + T_f s}\right) \tag{6}$$

功放模块中一阶低通环节的传递函数为:

$$G_a(s) = I_X(s)/I(s) = K_a/(s + a) \tag{7}$$

由式(4)、(6)、(7)可得:

$$F_X(s) = K_X \cdot X(s) + K_i \cdot I_X(s) = K_X \cdot X(s) + \frac{K_a K_p E(s)}{(s + a)}\left(1 + \frac{1}{T_i s} + \frac{T_d s}{1 + T_f s}\right) \tag{8}$$

磁悬浮飞轮转速变化以及转速控制由无刷直流电机提供。主被动磁悬浮飞轮无刷直流电机采用星型三相绕组结构以及 BUCK DC - DC 变换器和三相全桥的组合驱动控制方法,其拓扑结构如图 2 所示。

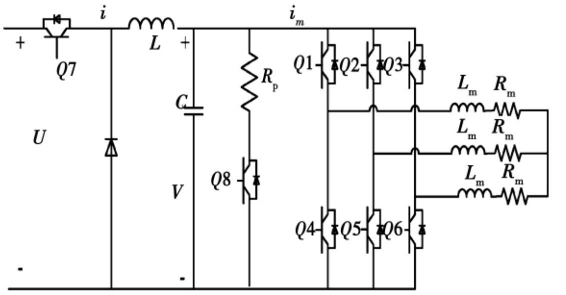

图 2　电机拓扑结构图

Fig. 2 Topological structural drawing of the motor

假设电机三相定子绕组对称,绕组电阻、电感值相同,且三相反电动势波形完全一致,并且半波对称,根据基尔霍夫电压定律和牛顿第二定律,建立主被动磁悬浮电机控制系统的模型为:

$$\begin{cases} C\dfrac{\mathrm{d}V}{\mathrm{d}t} = i - i_m \\ L\dfrac{\mathrm{d}i}{\mathrm{d}t} = Uu_1 - V \\ J\dfrac{\mathrm{d}\omega}{\mathrm{d}t} = K_T i_m - B\omega - T_d \\ L_m\dfrac{\mathrm{d}i_m}{\mathrm{d}t} = V - \dfrac{30K_e}{\pi p L_m}\omega - R_m i_m \end{cases} \tag{9}$$

式中: i—控制量输入; V—Buck 变换器的输出电压; i_m—飞轮电机电枢电流; p—飞轮电机转子磁极的极对数; ω—飞轮转速; T_d—随机扰动力矩; U—电源电压; u_1—控制输入; K_T—飞轮电机电磁力矩系数; J—飞轮转子的转动惯量; B—阻尼系数; L—Buck 变换器滤波电感; C—Buck 变换器滤波电容; L_m—绕组电感; R_m—绕组电阻。

电机采用速度环、电流环双闭环 PI 控制器,速度环 PI 控制器传递函数为:

$$G(s) = I_1(s)/E(s) = K_p(1 + 1/T_i s) \tag{10}$$

式中: $e = \Delta\omega = \omega_r - \omega$,$\omega_r$—电机参考转速,$\omega$—Hall 传感器测量的电机实际转速。电流环 PI 控制器传递函数为:

$$G_1(s) = U(s)/E_1(s) = K'_p(1 + 1/T_i s) \tag{11}$$

式中: $e_1 = \Delta I = i - i_1$,i—电机绕组参考电流,i_1—实际电流。

由式(9)、(10)、(11)可得:

$$U(s) = K'_p\left(1 + \frac{1}{T_i s}\right)\left[K_p \cdot E(s)\left(1 + \frac{1}{T_i s}\right) - I(s)\right] \tag{12}$$

?1994-2018 China Academic Journal Electronic Publishing House. All rights reserved.　http://www.cnki.net

2　控制器的设计与实现

主被动磁悬浮飞轮集成数字控制系统主要包括磁轴承控制模块、电机控制模块、模拟信号调理模块、磁轴承、电机功率放大模块和外扩存储模块。其原理如图 3 所示。磁轴承控制模块主要实现对主动磁轴承的控制，包括 DSP 模块和 FPGA 模块，DSP 模块主要实现磁轴承的控制算法处理、转速计算等功能，FPGA 模块主要进行转速计数以及磁轴承位移和电流信号的采样，并对 DSP 模块返回的控制量进行 PWM 调制。电机控制模块主要实现对无刷直流电机的控制，包括 DSP 和 FPGA 模块，FPGA 模块对电机绕组电流进行采样并对控制电流进行 PWM 调制，同时生成电机运行所需要的换向信号，DSP 模块主要实现电机电流环和转速环的控制算法。功率放大模块将磁轴承以及电机控制模块产生的控制量进行功率放大，使其具有足够大的功率驱动电机、磁轴承。模拟信号调理模块对磁轴承的位移传感器信号进行偏置、放大、滤波处理，对电机 Hall 信号进行滤波处理，处理过的信号分别输出至磁轴承控制模块和电机控制模块。

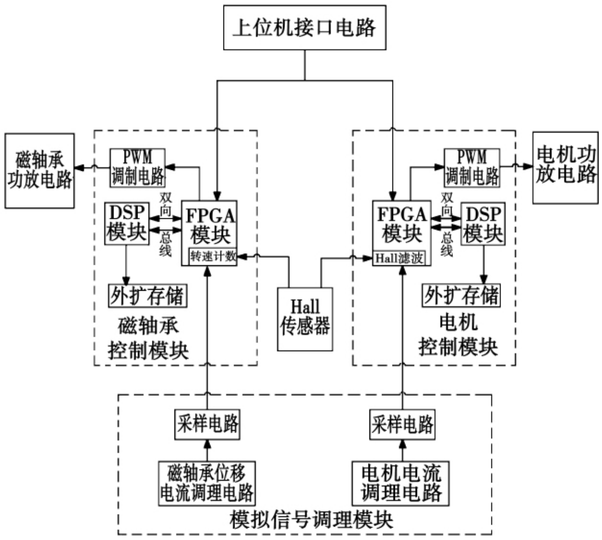

图 3　主被动飞轮集成控制系统原理框图

Fig. 3 Schematic block diagram of a driving and driven flywheel integrated control system

磁轴承控制算法：位移传感器测得的转子位移信号和磁轴承转子参考位移作差后得到的位移误差值 e 传给 PID 控制算法模块，经过磁轴承 PID 控制算法计算所得的电流信号 I 和电流传感器测得的磁轴承线圈电流信号 I_1 作差，得到的差值 e_1 即为控制电流，经过功率放大电路后输出至磁轴承线圈产生电磁力对转子系统进行控制。

电机控制算法：电机的参考转速信号 ω_r 和 Hall 传感器实测的电机转速信号 ω 作差后的转速误差信号 e 传给电机速度环 PI 控制器，经过速度环 PI 控制算法计算所得的电流信号 I 和电流传感器测得的电机绕组电流信号 i 作差，得到差值 e_1 输入至电流环控制器，电流环 PI 控制算法计算后得到电机绕组电压信号 U，经过功率放大电路后输出至电机绕组，进而对电机部分进行控制。

3　实验结果分析

为了验证磁悬浮轴承的控制效果，采用 TMS320C31 + FPGA 一体化数字控制器，以北京航空航天大学研制的主被动磁悬浮飞轮原理样机为实验对象，实验原理样机如图 4 所示，磁悬浮飞轮额定转速 5 000 r/min，在额定转速下输出角动量为7 N·m。

图 4 主被动磁悬浮飞轮原理样机

Fig. 4 Prototype of a driven and driving magnetically levitated flywheel

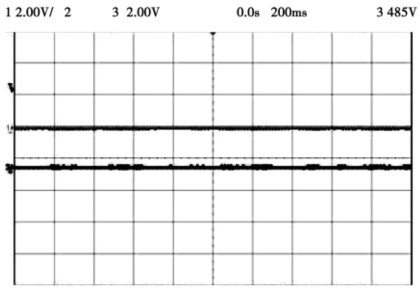

图 5　磁悬浮飞轮静浮实验结果

Fig. 5 Test results of the static levitation of a magnetically levitated flywheel

?1994-2018 China Academic Journal Electronic Publishing House. All rights reserved.　http://www.cnki.net

首先测试磁悬浮飞轮静态悬浮时的控制精度，飞轮电机不工作，主动磁轴承对飞轮转子进行控制，使转子处在磁轴承保护间隙的中心位置。实验结果如图 5 所示，主被动磁悬浮飞轮在静态悬浮时，转子径向位移跳动量仅为 70 mV(26μm) 左右，约为保护间隙(峰 - 峰值约 8V) 的 8.7%，达到了较好的静态悬浮效果。

随后测试飞轮加速时磁轴承控制精度测试。在电机的作用下飞轮转子加速至额定转速，如图 6 所示，此时转子转速 v = 4 900 r/min，转子径向跳动量为 1.2 V(0.28 mm)，约为保护间隙的 15% 左右。在飞轮加速的过程中，磁轴承较好地控制了飞轮转子。

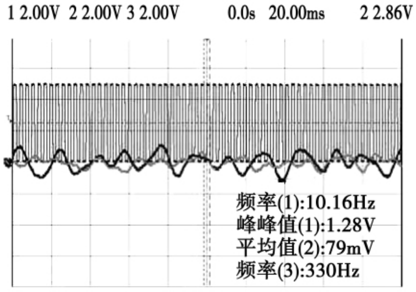

图 6　磁悬浮飞轮升速至额定转速时的实验结果

Fig. 6 Test results of a magnetically levitated flywheel when accelerated to the rated speed

当飞轮转子加速至额定转速时，飞轮电机停止工作，飞轮转子进行自由降速，通过测试飞轮降速特性来反映控制系统的控制效果，降速功耗曲线测试结果如图 7 所示。由图中曲线可以看到，磁悬浮飞轮以额定转速工作时，磁轴承系统功耗为 5.5 W 左右，达到了磁轴承控制系统低功耗的要求。

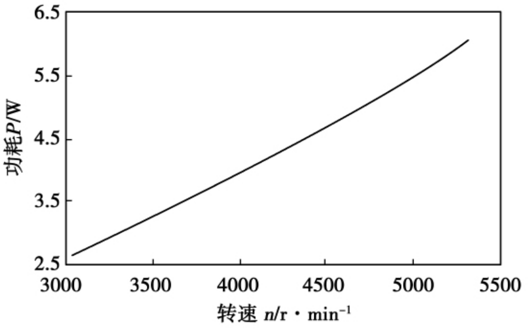

图 7　主被动磁悬浮飞轮降速功耗曲线

Fig. 7 Speed reduction power consumption of a driven and driving magnetically levitated flywheel

4　结　论

设计了一种基于 TMS320C31 + FPGA 的主被动磁悬浮飞轮数字控制器，并且对控制效果进行了实验验证。实验结果表明，磁悬浮飞轮在静态悬浮以及加速至额定转速时，转子的跳动量都达控制精度的要求，实现了磁轴承控制系统的高精度控制。飞轮工作在额定转速时，磁轴承系统功耗为 5.5 W，达到了磁轴承控制系统低功耗的要求。

参考文献：

[1] HAWKINS L A. Analysis and test of a magnetic bearing energy storage flywheel with gain - scheduled MIMO control [C\] /Proceeding of ASME Turbo Expo，Munich，Germany: IGTI，2000: 1 - 8.

[2] 孙津济，房建成，王　曦，等. 一种新型结构的永磁偏置径向磁轴承[J]. 电工技术学报，2009，24(11)：1 - 2.
SUN Jin-ji，FANG Jian-cheng，WANG Xi，et al. Permanent magnetic offset radial magnetic bearing with a new structure [J]. Transactions of China Electrotechnical Society，2009，24(11)：1 - 2.

[3] 刘　虎，房建成，刘　刚. 基于磁悬浮动量轮微框架能力的卫星滚动——偏航姿态稳定控制研究[J]. 宇航学报，2010，31(4)：3 - 4.
LIU Hu，FANG Jian-cheng，LIU Gang. Study of the stability control of a satellite rolling-yawed gesture based on the tiny framework capacity of a magnetically levitated momentum wheel [J]. Journal of Astronautics，2010，31(4)：3 - 4.

[4] MICHAEL SCHARFE. Design and development of a compact magnetic bearing momentum wheel for micro and small satellites [J]. Dreden University of Technology，Institute of Precision Engineering.

[5] 史光辉. 卫星对地观测高分辨率光学系统和设计问题[J]. 光学精密工程，1999，7(1)：16 - 24.
SHHI Guang-hui. A high resolution optic system for observation of the Earth from a satellite and its design problems [J]. Optic precision engineering，1999，7(1)：16 - 24.

[6] 房建成，孙津济. 一种磁悬浮飞轮用新型永磁偏置径向轴承[J]. 北京航空航天大学学报，2006，32(11)：1304 - 1307.
FANG Jian-cheng，SUN Jin-ji. A new type permanent offset radial bearing destined for magnetically levitated flywheels [J]. Journal of Beijing University of Aeronautics and Astronautics，2006，32(11)：1304 - 1307.

[7] 曹　洁. 电磁轴承系统位移传感器的分析与研究[J]. 传感器技术，2001，12: 9 - 11.
CAO Jie. Analysis and study of a displacement sensor for magnetic bearing systems [J]. Sensor technology，2001，12: 9 - 11.

[8] 许德章. 电涡流传感器信号调理电路的设计[J]. 自动化仪表，1998，16(6)：37 - 42.
XU De-zhang. Design of a circuit for regulating the signals of an eddy current sensor [J]. Automation instruments，1998，16(6)：37 - 42.

[9] 董淑成，房建成，俞文伯. 基于 PID 控制的主动磁轴承-飞轮转子系统运动稳定性研究[J]. 宇航学报，2005，26(3)：296 - 300.
DONG Shu-cheng，FANG Jian-cheng，YU Wen-bo. Study of the movement stability of a driven magnetic bearing-flywheel rotor system based on the PID control [J]. Journal of Astronautics，2005，26(3)：296 - 300.

?1994-2018 China Academic Journal Electronic Publishing House. All rights reserved.　http://www.cnki.net

ticle colony algorithm

双室热保护法测真空绝热板导热系数的装置及实验研究 = **Device for Measuring the Heat Conduction Coefficient of a Vacuum Insulation Plate By Using a Dual-chamber Heat Protection Method and Its Experimental Study** ［刊，汉］ KAN An-kang, HAN Hou-de (College of Merchant Ships, Shanghai Maritime University, Shanghai, China, Post Code: 201306) // Journal of Engineering for Thermal Energy & Power. – 2011, 26(6). –751 ~755

The traditional plate heat protection method for testing the heat conduction coefficient of a vacuum insulation plate (VIP) is limited by the dimensions of a VIP and affected by the heat bridge effect, thus, there exist certain demerits. The authors introduced a principle for determining the heat conduction coefficient of a VIP by using a dual-chamber heat protection method and designed a testing device. With the outer chamber serving as a heat protection device and the inner chamber serving as a testing and heating device, the heat conduction coefficient of the VIP was tested under a steady state. The device is not limited by the dimensions of the VIP with the heat bridge effect being reduced. The authors also analyzed the factors influencing the test results and the theoretical error. The test result was relatively precise when compared with the calibrated value. The device under discussion can be used for testing the heat conduction coefficient of a VIP before it leaves the works and inspecting the aging degree of any used VIP. **Key words**: vacuum insulation plate (VIP) , dual-chamber heat protection method, heat conduction coefficient, testing technique

基于TMS320C31 + FPGA 数字控制器的主被动磁悬浮飞轮一体化控制 = **Integrated Control of a Driving and Driven Magnetically Levitated Flywheel Based on a TMS320C31 + FPGA (Field-programmable Gate Array) Digital Controller** ［刊，汉］ ZHANG Fu-xin, LI Guang-jun, LIU Gang, et al (College of Instrumentation Science and Optoelectronic Engineering, Beijing University of Aeronautics and Astronautics, Beijing, China, Post Code: 100191) // Journal of Engineering for Thermal Energy & Power. – 2011, 26(6). –756 ~759

In the light of the demands for a low power consumption, high reliable and integrated driving and driven magnetically levitated flywheel with a driven control in three degrees of freedom along the axial direction and a driving control in two degrees of freedom along the radial direction, integrated and designed was its controller. Firstly, a mathematical model was established for the driving magnetic bearing with proper control tactics being chosen. On this basis, an integrated digital control system with DSP + FPGA serving as the core, including a signal modulation, outer storage, driving and power amplification module, was presented and experimentally verified. The test results show that when the flywheel is levitated in a static state, the radial runout of the rotor is around 70 mV, about 8.7% of the protection clearance (the peak-peak value is about 8 V) . When the flywheel is accelerated to its rated speed, the radial runout of the rotor is around 1.2 V, around 15% of the protection clearance. When operating at the rated speed, the power consumption of the magnetic bearing system of the magnetically levitated flywheel is only 5.5 W, thus meeting the requirements for the performance of the flywheel. **Key words**: driving and driven magnetic levita-

?1994-2018 China Academic Journal Electronic Publishing House. All rights reserved. http://www.cnki.net

ted flywheel, magnetic bearing, integrated controller, DSP (digital signal processing), FPGA (Field-programmable gate array)

进气管通道直径对直接内部甲烷蒸汽重整性能的影响 = **Influence of the Passage Diameter of an Inlet Pipe on the Direct Steam Reforming Performance of Inner Methane** ［刊，汉］ YU Jian-guo, WANG Yu-zhang, WENG Shi-lie (Education Ministry Key Laboratory on Power and Mechanical Engineering, College of Mechanical and Power Engineering, Shanghai Jiaotong University, Shanghai, China, Post Code: 200240) // Journal of Engineering for Thermal Energy & Power. – 2011, 26(6). –760 ~ 763

Steam reforming boasts very obvious edges for utilizing methane and other fuels in solid oxide fuel cells. Based on the commercial software CFD and various programs developed for the complicated physical process and electrochemical reactions relating to multi-component flow and dispersion, heat and mass transfer, electrochemical reactions and electric current field inside the porous media of fuel cells etc., numerically calculated was the steam reforming process of methane inside a planar-electrode-support solid fuel cell (PES-SOFC) with distributions of such parameters as various gas component mole fraction, temperature, temperature gradient and output voltage in the fuel cell under different diameters of the exhaust pipe being obtained. The calculation results show that when the passage diameter is 0.0045 m, the output voltage is the highest, reaching 0.4923 V and in the meantime, when such a diameter ranges around 0.0045 – 0.005 m, a relatively optimized temperature distribution can be guaranteed. **Key words**: solid oxide fuel cell, reforming, passage diameter, voltage

城市污泥混掺小麦秸秆制备活性炭的研究 = **Study of the Preparation of Activated Carbon By Using Urban Sludge Mixed With Wheat Straws** ［刊，汉］ GUO Bin, LI Xu-guang, LIU Ren-ping, et al (College of Environemnt Science and Engineering, Hebei University of Science and Technology, Shijiazhuang, China, Post Code: 050018) // Journal of Engineering for Thermal Energy & Power. –2011, 26(6). –764 ~ 767

With two kinds of solid waste, urban sludge and wheat straw, serving as the main raw materials and zinc chloride being chosen as the activation agent, through a orthogonal test, optimized were the technological conditions for preparing hybrid activated carbon and performed were an analysis of the specific surface area, hole diameter distribution, iodine adsorption value, SEM and FTIR relating to the specimen of the activated carbon. It has been found that the optimum technological parameters for preparation of activated carbon can be listed as follows: immersion ratio 2:1, activation time duration 60 minutes, raw material ratio 1:1 and activation temperature 500 ℃. Under such conditions, the specific surface area of the activated carbon thus obtained can be as high as 1034.431 m^2/g, iodine value 804.216 mg/g and production rate 41.28%. The volumes of the big, intermediate and small holes inside the activated carbon are 0.317 mL/g, 0.257 mL/g and 0.742 mL/g respectively with the mean hole diameter being 2.32 nm. In the IR (infrared) peaks, C = C, O – H, C – OH and C – N represent the surface function group of the activated carbon. **Key words**: urban sludge, wheat straw, activated carbon, orthogonal test

?1994-2018 China Academic Journal Electronic Publishing House. All rights reserved. http://www.cnki.net